energies

MDPI

Article

Performance Evaluation of Coupled Thermal Enhancement through Novel Wire-Wound Fins Design and Graphene Nano-Platelets in Shell-and-Tube Latent Heat Storage System

Zakir Khan [1,2] and Zulfiqar Ahmad Khan [1,*]

[1] NanoCorr, Energy and Modelling (NCEM) Research Group, Department of Design & Engineering, Bournemouth University, Talbot Campus, Fern Barrow, Poole, Dorset BH12 5BB, UK; zakkhan2572@gmail.com

[2] School of Mechanical & Manufacturing Engineering (SMME), National University of Sciences & Technology (NUST), Sector H-12, Islamabad 44000, Pakistan

* Correspondence: zkhan@bournemouth.ac.uk; Tel.: +44-1202-961645

Abstract: Technological development in latent heat storage (LHS) systems is essential for energy security and energy management for both renewable and non-renewable sources. In this article, numerical analyses on a shell-and-tube-based LHS system with coupled thermal enhancement through extended fins and nano-additives are conducted to propose optimal combinations for guaranteed higher discharging rate, enthalpy capacity and thermal distribution. Transient numerical simulations of fourteen scenarios with varied combinations are investigated in three-dimensional computational models. The shell-and-tube includes paraffin as phase change material (PCM), longitudinal, radial and wire-wound fins and graphene nano-platelets (GNP) as extended fins and nano-additives, respectively. The extended fins have demonstrated better effectiveness than nano-additives. For instance, the discharging durations for paraffin with longitudinal, radial and wire-wound fins are shortened by 88.76%, 95.13% and 96.44% as compared to 39.33% for paraffin with 2.5% GNP. The combined strengths of extended fins and nano-additives have indicated further enhancement in neutralising the insulative resistance and stratification of paraffin. However, the increase in volume fraction from 1% to 3% and 5% is rather detrimental to the total enthalpy capacity. Hence, the novel designed wire-wound fins with both base paraffin and paraffin with 1% GNP are proposed as optimal candidates owing to their significantly higher heat transfer potentials. The proposed novel designed configuration can retrieve 11.15 MJ of thermal enthalpy in 1.08 h as compared to 44.5 h for paraffin in a conventional shell-and-tube without fins. In addition, the proposed novel designed LHS systems have prolonged service life with zero maintenance and flexible scalability to meet both medium and large-scale energy storage demands.

Keywords: thermal energy storage (TES); latent heat storage (LHS); graphene nano-platelets; solidification; heat transfer enhancement; shell-and-tube heat exchanger

Citation: Khan, Z.; Khan, Z.A. Performance Evaluation of Coupled Thermal Enhancement through Novel Designed Wire-Wound Fins and Graphene Nano-Platelets in Shell-and-Tube Based Latent Heat Storage System. *Energies* **2021**, *14*, 3743. https://doi.org/10.3390/en14133743

Academic Editor: Claudio Mele

Received: 20 May 2021
Accepted: 17 June 2021
Published: 22 June 2021

1. Introduction

The rapidly depleting non-renewable sources and the associated ecological and environmental threats have prompted to bring about advancement in energy management and to switch reliance onto renewable sources to ensure long-term energy security. In spite of increasing global trend to capitalise on renewable sources, its total contribution is less than one-third in global energy demand [1,2]. Therefore, the innovation and development in energy technologies are crucial for sustainable growth towards a carbon neutral world [3]. Recent development in energy storage systems have inculcated broad-ranging advantages, such as better load management and peak shaving, damping energy fluctuations, improving energy security and reliability. In addition, energy storage systems are

essential in promoting an increased penetration of renewable energy in the global energy mix [4].

In the past decade, thermal energy storage (TES) systems have noticed an increased attention from scientists and engineers as a potential candidate to contribute to sustainable global energy demands. Latent heat storage (LHS) systems with a broad range of materials in sub-zero and low-medium-high temperature ranges along with higher energy storage capacity and easier integration into industrial, commercial and domestic setups have been regarded as a promising technological solution [5–7]. However, the large-scale employment of LHS systems and their projected penetration into the global energy mix are hindered by the insulative nature of phase change materials (PCM), which are utilised as energy storage medium. To counter the insulative nature, several methods have been investigated, such as the geometrical configuration of the heat exchanger, addition of extended fins, nano-additives, metal-matrix, micro- and macro-encapsulation [7–9].

Shell-and-tube dominates the global heat exchanger market due to its superior thermo-physical performance, compact and robust design, easier upgradation and integration to wider practical applications [10,11]. Similarly, the inclusion of a variety of extended fins to shell-and-tube-based LHS systems were previously reported. Essa et al. [12] conducted experimental investigations on the effectiveness of helical and longitudinal fins in a solar-based heat pipe system. It was reported that the discharging efficiency for helical fins at higher flow rates were 15.13% higher as compared to longitudinal fins. However, the discharging efficiency for helical fins at lower flow rates demonstrated a relative reduction of 3.69%, owing to weaker natural convection in paraffin at lower flow rates. Gil et al. [13] conducted experimental investigations to evaluate the impact of transversal squared fins on the effective thermal conductivity of a pilot plant-scale LHS system. It was reported that the effective thermal conductivity improved by 25.83% with fins as compared to the no-fins setup. Likewise, the comparative analysis of longitudinal and triangular fins in a horizontally oriented shell-and-tube were performed by simulating two-dimensional computational domains [14,15]. It was reported that triangular fins indicated superior performance compared to longitudinal fins. However, the design constrains were ignored, which caused incomparable total energy capacity. Similarly, the impact of solid and perforated radial fins on thermal enhancement of a vertically oriented shell-and-tube was experimentally studied in [16]. It was reported that perforated radial fins promoted natural convection and hence, the thermal performance was improved by 7%.

Likewise, Anish et al. [17] conducted two-dimensional numerical investigations on a horizontal shell-and-tube with multi-tube and longitudinal fins-based LHS system. It was noticed that the increase in the number of multi-tubes from 5–9, number of fins from 2–6 per tube and length of fins from 6–15 mm improved the thermal performance by 40%, 8% and 31%, respectively. However, it compromised the storage capacity and suppressed the buoyancy-driven natural convection. Lu et al. [18] experimentally examined multi-tube with helical fins in a vertical shell-and-tube. It was construed that, although the multi-tube with helical fins significantly improved the melting and solidification rates, the optimum effectiveness in the solidification process was curtailed by insulative solidified layers of PCM. Ge et al. [19] conducted two-dimensional numerical investigations on a multi-tube with optimised topology and longitudinal fins in a horizontally oriented shell-and-tube. It was reported that the topology-optimised fins indicated 57.1% improvement over longitudinal fins. However, the length of the topology-optimised and longitudinal fins was not constrained, which could potentially lead to uncertain results of the comparative analysis. Khan et al. [20] conducted a parametric evaluation focusing on the number and orientation of the multi-tube, along with geometrical sizing and material of longitudinal fins in a vertically oriented shell-and-tube-based LHS system. An optimised novel design comprising 21 copper-based multi-tubes and 76 longitudinal fins in a shell container was proposed. Later on, the proposed optimal design was experimentally analysed for charging and discharging cycles at the range of operating conditions to gauge its robustness

and effectiveness for potential practical applications [21–23]. It was observed that the proposed optimal design was effective in charging 14.36 MJ of thermal enthalpy in 3.12 h and discharging 12.09 MJ in 1.5 h, respectively. Moreover, the significant influence of natural convection on the temperature distribution in the shell container and subsequent impacts on the charging/discharging rates were discussed. It is deduced from the literature that extended fins have potentials to bring about significant thermal enhancement in the shell-and-tube. However, the disadvantage associated with extended fins include the overall weight increase of LHS system.

To moderate the downside related to extended fins, the addition of nano-additives has been considered as a promising alternative [24,25]. However, the continuous charging and discharging cycles of LHS system can cause agglomeration and sedimentation issues for nano-additives with relatively higher density than the base PCM. Moreover, besides improving the thermal conductivity through nano-additives, the dynamic viscosity would also be influenced, which could be detrimental for natural convection and thermal distribution within the shell container [26–28]. Therefore, the carbon allotropes with optimal concentration are deemed as appropriate nano-additives because of their lower density, better particles distribution and extended suspension in the base PCM. Furthermore, the combination of extended fins and nano-additives would potentially generate significant thermal enhancement in LHS systems.

Goodarzi et al. [29] conducted experimental investigations on thermofluidic characteristics of graphene oxide nano-platelets based nano-PCM in a vertical annular heat exchanger. It was reported that the heat transfer performance can be augmented by increasing the values of parameters, such as concentration of graphene oxide, inlet temperature of heat transfer fluid and heat flux. Yarmand et al. [30] prepared and analysed hybrid GNP-Pt-based nano-PCM. It was noticed that with the inclusion of 0.1 wt% of hybrid nano-additives, the thermal conductivity and viscosity can be improved by 17.77% and 33%, respectively. Likewise, Goodarzi et al. [31] conducted numerical investigations on the thermal performance enhancement of a heat exchanger with varied cross-sections, such as circular, trapezoidal and square and hybrid GNP-Ag based nano-PCM. Li et al. [32] reported that the thermal conductivity and heat transfer coefficient of a heat exchanger can be augmented by 14% and 73% with inclusion of 0.1 wt% of carbon nano-additives to base acetone.

Sarani et al. [33] conducted numerical investigations on longitudinal fins and copper oxide on the discharging cycle of paraffin in a two-dimensional computational domain of shell-and-tube. It was noticed that, compared to paraffin with longitudinal fins, the inclusion of copper oxides reduced the solidification duration from 3.17 h to 1.77 h. Hosseinzadeh et al. [34] investigated the combined impact of longitudinal fins and hybrid MoS_2-Fe_3O_4-based nano-additives on the discharging cycle in a two-dimensional computational model of a horizontal triplex tube-based LHS system. It was reported that the solidification rate was improved by 14% for combined enhancement as compared to the individual enhancement of 9% for longitudinal fins and 4% for nano-additives, respectively. Sheikholeslami et al. [35] examined the influence of v-shaped extended fins and copper oxide as nano-additives on the solidification process by simulating a two-dimensional computational model of a vertical LHS unit. It was reported that the combined effect of extended fins and nano-additives expedited the solidification process. However, as similar to the majority of the published literature, the impact of natural convection on the solidification process was not considered. Mahdi and Nsofor [36] investigated the solidification performance of nano-PCM with longitudinal fins and aluminium oxide-based nano-additives in a horizontally oriented triplex tube-based LHS system. It was noted from two-dimensional numerical simulations that the solidification duration was reduced by 33.4% for coupled enhancement as compared to 31.5% reduction for fins alone. Furthermore, Singh et al. [37] experimentally investigated the discharging behaviour of nano-

PCM with radial fins and GNP as nano-additives in a vertical shell-and-tube. It was reported that the discharging rate was improved by 49% for coupled enhancement as compared to 26% for individual enhancement through radial fins.

It can be noticed that coupled enhancement through extended fins and nano-additives have significant potential to upgrade the melting and solidification performance of LHS systems. However, it can also be deduced that the literature lacks novel geometrical designs for shell-and-tube with extended fins to capitalise on the strengths and overcome the limitations incurred by conventional longitudinal and radial fins. Furthermore, the published literature has primarily reported two-dimensional numerical simulations and lacks three-dimensional transient simulations which could provide more detailed and relatively accurate thermo-physical performance evaluation of LHS systems. Lastly, the literature also lacks the comparative numerical analyses on solidification behaviour of carbon allotropes-based nano-PCM with varied volume fractions and varied geometrical designs of extended fins in three-dimensional computational domains.

To address the mentioned gaps in the literature, a novel designed shell-and-tube with wire-wound fins and graphene nano-platelets (GNP) with varied volume fractions is numerically investigated through transient simulations on discharging cycles in three-dimensional computational domains. In addition, the comparative analyses are conducted by simulating the discharging cycles for fourteen varied scenarios including base PCM and nano-PCMs in a shell-and-tube with a standard plain tube and a tube with longitudinal, radial and wire-wound fin configurations. In our previous publication [38], the influence of coupled enhancement on charging cycles of LHS systems were discussed. Whereas this article is focused on understanding and investigating the impact of coupled enhancement on discharging cycles of LHS systems, which has not been reported in the literature. Furthermore, this article will propose optimal combinations of coupled enhancement for the LHS system which will generate higher discharging rate, higher energy capacity and better heat distribution to ensure long-term practical utilisation in wider applications.

2. Numerical Modeling

2.1. Physical Models

In order to acquire optimal performance enhancement in a shell-and-tube-based LHS system, the coupled enhancement through extended fins and nano-additives are introduced and investigated in three-dimensional computational domains. The physical models of coupled enhancements include longitudinal, radial and wire-wound fins with nano-PCMs in shell-and-tube configuration, as illustrated in figure number 1 in [38]. The motive behind transient simulations of coupled enhancement in three-dimensional computational domains is to propose an optimal combination that can guarantee the retrieval of higher enthalpy capacity at higher discharging rate, better thermal distribution in the shell container and higher heat transfer performance. Moreover, the transient simulations empower to track and gauge the phase front propagation and the impact of natural convection on the solidification process in the respective coupled enhancement scenario.

As illustrated in figure number 1 in [38], the physical models of shell-and-tube with multiple passes and tubes with longitudinal, radial and wire-wound fins conform to geometrical constrains and symmetries. To reduce the computational cost and time, the computational domain for each extended fin scenario is chosen by adhering to geometrical symmetries of tube passes in the shell container. To perform a comparative analysis, the length, thickness and volume occupation of extended fins are constrained to 50.8 mm, 1 mm and 93.5 cm^3, respectively. To comply with the assigned constrains, the longitudinal fins configuration comprises 8 vertical fins with symmetrical distribution across the tube diameter. Hence, the longitudinal fins are 45° apart to each other. In the case of the radial fin configuration, the assigned constrains are realised by 8 radial fins with symmetrical distribution across the tube height. Thus, the radial fins are distanced by 30 mm to each other. Likewise, in the case of the wire-wound fins configuration, the assigned constrains

are satisfied with a symmetrical distribution of 50 fins per loop across the tube diameter and 23 loops across the tube height. The radial distribution for wire-wound fins makes 7.2° to each other and the vertical distribution of the loop centres are at a 10-mm distance to each other. Furthermore, the external diameter and height of all computational domains are identical at 148 mm and 230 mm, respectively.

A shell-and-tube with extended fins is made of copper due to its favourable characteristics including easier welding and bending, higher thermal conductivity and good compatibility with nano-PCMs. Paraffin (RT44HC) is chosen as base thermal storage material for the reasons of excellent thermo-physical stability and reliability, higher heat storage capacity and good compatibility with metals and nano-additives [7,39]. Likewise, GNP are selected as nano-additives because of their desired potentials including higher thermal conductivity, lighter density, excellent emulsification and longer suspension in base paraffin [27]. Nano-PCM occupy the volume in the shell container, whereas water is employed as the heat transfer fluid (HTF) to flow in the tube and retrieve the thermal enthalpy from nano-PCM. Table 1 provides the thermal and physical properties of materials involved. Moreover, Table 2 provides the list of fourteen couple enhancement scenarios involving both paraffin and nano-PCMs in the tube without and with extended fins. For comparative analyses, the packing factor (P.F) ratio provides a rationale to compare coupled enhancement scenarios with identical values.

Table 1. Thermal and physical properties of materials involved in coupled enhanced LHS systems are provided below in the table and have been obtained from suppliers [39,40] and are in the public domain.

	Units	Paraffin	Copper	GNP
Density	kg/m^3	800 (s), 700 (l)	8920	400
Thermal conductivity	W/m	0.2	400	3000
Specific heat capacity	kJ/kg K	2.0	380	643
Latent heat capacity	kJ/kg	255	-	-
Phase change temperature	°C	41–44	-	-

Table 2. Number of coupled enhancement cases and their respective packing factor value.

Case No.	Extended Fins	PCM	P.F *
1	No-fins	Paraffin	1
2	No-fins	Nano-PCM—2.5% GNP	0.975
3	Longitudinal fins	Paraffin	〃
4	Radial fins	Paraffin	〃
5	Wire-wound fins	Paraffin	〃
6	Longitudinal fins	Nano-PCM—1% GNP	0.965
7	Radial fins	Nano-PCM—1% GNP	〃
8	Wire-wound fins	Nano-PCM—1% GNP	〃
9	Longitudinal fins	Nano-PCM—3% GNP	0.945
10	Radial fins	Nano-PCM—3% GNP	〃
11	Wire-wound fins	Nano-PCM—3% GNP	〃
12	Longitudinal fins	Nano-PCM—5% GNP	0.925
13	Radial fins	Nano-PCM—5% GNP	〃
14	Wire-wound fins	Nano-PCM—5% GNP	〃

* $\varphi_{P.F} = {}^{V_{PCM}}/_{V_S}$

2.2. Governing Equations and Computational Assumptions

In order to conduct transient numerical simulations on coupled enhancement scenarios in three-dimensional computational domains, the following assumptions are implemented to achieve reduced computational complexity, cost and time:

- During the solidification process, the volumetric shrinkage of nano-PCMs is neglected;
- Exterior boundaries of computational domains are assigned with adiabatic conditions;
- A fully developed flow condition with negligible temperature variations in HTF is assumed, and hence, a constant wall temperature is assigned to the tube boundaries;
- Nano-PCMs are incompressible and natural convection is calculated by implementing the Boussineq approximation.

The numerical methodology is developed for discharging cycles of coupled enhancement scenarios by considering the computational assumptions. The mass, momentum and energy conservation equations are:

$$\frac{\partial \rho}{\partial t} + \nabla \cdot \left(\rho \vec{V}\right) = 0 \tag{1}$$

$$\frac{\partial \left(\rho \vec{V}\right)}{\partial t} + \rho \vec{V} \cdot \left(\nabla . \vec{V}\right) = -\nabla P + \mu \nabla^2 \cdot \vec{V} + \rho \beta \vec{g}(T - T_{REF}) + \frac{C(1-f)^2}{(f^3 + \alpha)} \vec{V} \tag{2}$$

$$\frac{\partial (\rho H)}{\partial t} + \nabla \cdot \left(\rho H \cdot \vec{V}\right) = \nabla \cdot \left(\frac{k}{\rho C_P} \nabla H\right) + q \tag{3}$$

During the discharging cycle, the phase transformation from liquid-mushy-solid is evaluated by implementing the enthalpy-porosity method. It was observed from the literature that natural convection is usually neglected in the solidification process of the LHS system. In the current study, the influence of natural convection on the discharging cycle is computed by incorporating the Boussineq approximation [41] in the equation for momentum conservation (Equation (2)). Transient density variations with respect to temperature of nano-PCMs are considered for calculating the instantaneous natural convection and phase front propagation in a three-dimensional computational domain. During the phase transformation from liquid-mushy-solid, the enthalpy-porosity technique considers the mushy zone as a porous medium. The liquid fraction in mesh cells is associated with the porosity. Darcy's law for porous media [42] and momentum sink terms are included in the momentum conservation (Equation (2)) for measuring the liquid fraction and for damping phenomena caused by variations in velocities in the mushy zone, respectively. The damping amplitude during the liquid-solid transition is controlled by the morphological constant *C*, which has a functional value range from 10^5–10^7. A higher morphological constant value exhibits a sharper transition for mushy zone velocities to standstill as the liquid fractions progress from 1 to 0. Therefore, the numerical simulation results are equated with experimental results in [22] and the morphological constant of 10^6 is chosen for obtaining a good agreement. Likewise, the liquid fraction *f* is associated with instantaneous temperature *T* of nano-PCM, as follows:

$$f = \begin{cases} 0 & T < T_S \\ 1 & T > T_L \\ \dfrac{T - T_S}{T_L - T_S} & T_S \le T \le T_L \end{cases} \tag{4}$$

where T_S and T_L are solidus and liquidus temperatures of nano-PCM. Moreover, a small computational number ($\alpha = 10^{-3}$) is included in Equation (2) to intercept a division by zero. In the energy conservation statement (Equation (3)), the overall enthalpy *H* is the aggregation of sensible and latent enthalpies and can be calculated as follows:

$$H = h_{REF} + \int_{T_{REF}}^{T} C_P dT + fL \tag{5}$$

where the 1st term on right-hand side of Equation (5) illustrates the reference enthalpy of nano-PCM at reference temperature (T_{REF} = 273.15 K). Similarly, the 2nd and 3rd terms

demonstrate the sensible and latent enthalpies, respectively. In case of coupled enhancement scenarios, the transient changes in thermal and physical characteristics of nano-PCMs, comprising base paraffin and GNP as nano-additives, are estimated by implementing the formulas for the mixture of two components, as given below [43]:

$$\rho_{nPCM} = \Phi_{VC}\rho_{GNP} + (1 - \Phi_{VC})\rho_{PCM} \quad (6)$$

$$\beta_{nPCM} = \frac{\Phi_{VC}\rho_{GNP}\beta_{GNP} + (1 - \Phi_{VC})\rho_{PCM}\beta_{PCM}}{\rho_{nPCM}} \quad (7)$$

$$C_{P,nPCM} = \frac{\Phi_{VC}\rho_{GNP}C_{P,GNP} + (1 - \Phi_{VC})\rho_{PCM}C_{P,PCM}}{\rho_{nPCM}} \quad (8)$$

$$L_{nPCM} = \frac{(1 - \Phi_{VC})\rho_{PCM}L_{PCM}}{\rho_{nPCM}} \quad (9)$$

Moreover, the Corcione semi-empirical model [44] is implemented to evaluate the transient variations in the dynamic viscosity by taking into account the particle size and volume fraction of GNP, and the instantaneous temperature. Transient variations in the dynamic viscosity of paraffin and nano-PCMs are calculated from Equations (10) and (11), as follows [44,45]:

$$\mu_{PCM} = 0.001exp\left(-4.25 + \frac{1790}{T}\right) \quad (10)$$

$$\mu_{nPCM} = \frac{\mu_{PCM}}{1 - 34.87(d_{GNP}/d_{PCM})^{-0.3}{\Phi_{VC}}^{1.03}} \quad (11)$$

$$d_{PCM} = 0.1\left(\frac{6M_W}{\pi N_A \rho_{PCM,O}}\right)^{0.333} \quad (12)$$

where d_{PCM} represents the equivalent diameter of paraffin and the diameter of GNP is equal to d_{GNP} = 6 nm [27,40]. Furthermore, the transient changes in the effective thermal conductivity of nano-PCMs are realised by implementing the semi-empirical model derived by Vajjha and Das [46]:

$$k_{nPCM} = \frac{k_{GNP} + 2k_{PCM} - 2(k_{PCM} - k_{GNP})\Phi_{VC}}{k_{GNP} + 2k_{PCM} + (k_{PCM} - k_{GNP})\Phi_{VC}}k_{PCM} + 5 \times 10^4 \zeta \rho_{PCM}\Phi_{VC}C_{P,PCM}\sqrt{\frac{\kappa_B T}{\rho_{GNP}d_{GNP}}}f(T, \Phi_{VC}) \quad (13)$$

$$f(T, \Phi_{VC}) = (2.8217 \times 10^{-2}\Phi_{VC} + 3.917 \times 10^{-3})\left(\frac{T_{nPCM}}{T_{REF}}\right) + (-3.0669 \times 10^{-2}\Phi_{VC} - 3.91123 \times 10^{-3}) \quad (14)$$

In Equation (13), the modulating parameters include the particle size and volume fraction of GNP, thermo-physical characteristics of both paraffin and GNP, instantaneous temperature and the Brownian motion of particles in liquidus nano-PCM. In Equation (13), the 1st term is the static contribution to k_{nPCM} which is derived from the Maxwell model [47], whereas the 2nd term accounts for the dynamic contribution including the Brownian motion.

2.3. Initial and Boundary Conditions

In the discharging cycle, the heat transfer between low-temperature water in the tube and high-temperature liquid nano-PCM in the shell container enables the phase change

from liquid-mushy-solid. To simulate the discharge cycle, the initial temperature of nano-PCM in the shell container is set to 62 °C, which guarantees an initial liquid state. Similarly, the inner wall of tube is set to 15 °C, which simulates the low-temperature municipal water [22]. The discharging cycle completes at instant when the entire volume of nano-PCM registers the temperature in solidus state.

2.4. Numerical Simulation Procedure

The finite volume method (FVM) is implemented to discretise the mass, momentum and energy equations for coupled enhancement scenarios in three-dimensional computational domains, as illustrated in Figure 1 in [38]. A pressure-based sequential algorithm is chosen for simulating the transient discharging cycle. The pressure-implicit with splitting of operators (PISO) algorithm is adopted for pressure-velocity coupling in the momentum equation (Equation (2)). The pressure staggering option (PRESTO) and second-order upwind schemes are considered for pressure corrections and spatial discretisation of the convective terms in Equations (2) and (3). The Green–Gauss theorem is employed for nodal-based spatial discretisation of gradients and derivatives. Moreover, the absolute convergence criterion for residuals in the governing equations are examined at each time step for values less than 10^{-6}. A first-order implicit time-stepping approach with fixed iterations is chosen for a stable solution of the transient discharging cycle. User-defined functions (UDF) are utilised to formulate temperature-dependent thermo-physical characteristics of nano-PCMs.

It is imperative for the accuracy and precision of the numerical results that the time-stepping and grid-resolution independency are established for the aforementioned coupled enhancement scenarios including the no-fins, longitudinal, radial and wire-would fins configurations. In the case of grid-resolution, the transient discharging simulations are conducted with fixed time-stepping (Δt = 1 s) for three varied mesh sizes of each computational domain. The liquid fractions for each scenario are matched and the grid-resolution independency with mesh sizes of 5.35×10^7, 3.70×10^7, 2.35×10^7 and 8.08×10^7 are established, respectively. Likewise, the time-stepping for all scenarios with their respective grid-resolutions are investigated with three different time steps of 0.1, 0.5 and 1 s. The liquid fractions response to the varied time-stepping are uniform, and hence, the time step of 1 s is chosen for reliable numerical results at lower computational cost [38].

To validate the numerical simulation results, the transient temperature plots from the discharging cycles in three-dimensional computational domains are compared with experimental data for paraffin with longitudinal fins in [22] and nano-PCM with 1% GNP in the shell-and-tube in [27], as illustrated in Figure 1. The computational domains for both scenarios are developed by considering their respective geometrical configurations, material characteristics, initial and boundary conditions for discharging cycles as described in [22,27]. The robustness and accuracy of the numerical simulations are validated by showcasing good agreement between the experimental and numerical temperature profiles. Mean absolute errors for both scenarios are computed to be 2.57% for Figure 1a and 2.87% for Figure 1b.

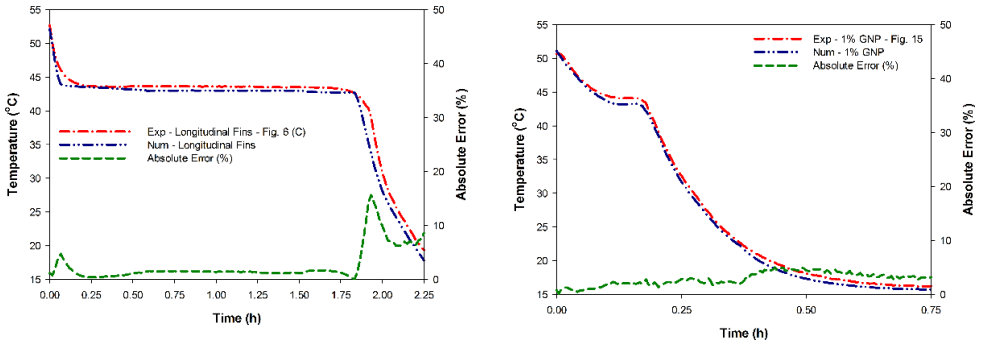

(**a**) (**b**)

Figure 1. Validation of the numerical model with experimental temperature profiles: (**a**) paraffin with longitudinal fins and (**b**) nano-PCM with 1% GNP in shell-and-tube configurations.

3. Results and Discussion

3.1. Discharging/Solidification Cycles

During the solidification process, the heat transfer between low-temperature water flowing in the tube and high-temperature liquid nano-PCM in the shell container can be categorised into three distinctive stages. In the initial stage, the higher temperature gradient enables the rapid extraction of thermal energy from liquid nano-PCM. Hence, the heat flux upsurges to reach its peak value. In this stage, the sensible portion of the overall enthalpy is discharged by liquid nano-PCM, the temperature decreases from 62 to 44 °C and the heat transfer is governed by both natural convection and conduction. In the second stage, the phase transition from liquid-mushy-solid originates as the nano-PCM begins to discharge the latent enthalpy. A solidified layer starts developing on the exterior fin of multi-tube passes, which thickens as the discharging cycle proceeds. The formation of the solidified layer coupled with the reduction in temperature gradient weakens the heat flux with a sharp decline and is followed by a gradual decrease until the completion of the second stage. In this stage, both natural convection and conduction influence the heat transfer; however, the dominance of conduction is noticed as the solidified layer thickens. In the discharging cycle, the second stage demands the longest duration to release the higher latent enthalpy of nano-PCM with relatively weaker heat flux as the temperature reduces from 44 to 41 °C. In the final stage, the sensible portion of the overall enthalpy is discharged by solidified nano-PCM, which follows the trend of gradual reduction in heat flux from the earlier second stage. It is due to the further reduction in temperature gradient and maximum resistance to heat transfer by the solidified layers. In this stage, conduction heat transfer is dominant and the temperature reduces from 41 to 15 °C.

In order to conduct the comparative thermal analysis of fourteen coupled enhancement scenarios, the transient numerical simulation of case 1 is chosen as benchmark. In case 1, paraffin without nano-additives and a tube without extended fins, having the packing factor equal to 1, is simulated in a three-dimensional computational domain. Figure 2 presents the temperature, total enthalpy and liquid fraction contours throughout the discharging cycle. The temperature contours are demonstrated in the top row, whereas the cross-sectional view of the temperature contours on the left and liquid fraction and total enthalpy on the right are illustrated in the bottom row. Moreover, the transient responses of velocity of phase front movement, liquid fraction, temperature, enthalpy, heat flux and heat transfer coefficient throughout the discharging cycle are provided in Figure 3.

In the earlier stages of the discharging cycle, the higher temperature gradient elevates the heat flux which results in a rapid discharge of sensible enthalpy. In this stage, the heat flux and mean velocity record their peak values of 3.279 kW/m^2 and 0.434 mm/s, as shown in Figure 3. In the second stage, the liquid paraffin in contact with exterior fin of the cold tube discharges the latent enthalpy and a phase change occurs from liquid–mushy–solid.

Figure 2 illustrates that, although the solidified layer thickness increases near the cold exterior fin of the tube, the thermal propagation is quite weak in the regions even at short distances from the solidified layers. It confirms the insulative nature of paraffin both in liquid and solid phases. Moreover, the upward movement of high-temperature liquid paraffin under the influence of buoyancy validates the influence of natural convection on the solidification process. It can be noticed from the contours that paraffin in the lower section of the shell container discharges the total enthalpy and undergoes a phase transition relatively quicker due to the temperature gradient established along the height of the shell container. However, the weaker thermal propagation and accumulation of liquid paraffin in upper section provide hurdles to the solidification process, and therefore, the duration to complete the discharging cycle increases. For instance, while discharging for 5, 10, 20, 30 and 40 h, the liquid fraction for paraffin in the entire computational domain is reduced to 0.611, 0.462, 0.269, 0.123 and 0.016, respectively. Likewise, the total enthalpy is reduced to 182.8, 141.8, 88.99, 49.26 and 13.28 kJ/kg, respectively. In the second stage, the solidified layer is controlled by conduction heat transfer and the liquid paraffin by natural convection. It is also noted that with the growth in the solidified layer, the velocity of liquid paraffin decreases, and hence, the heat transfer is dominated by conduction. In the final stages, the insulative nature of the solidified layer intensifies, and hence, the heat flux, liquid fraction and total enthalpy curves demonstrate a gradual logarithmic reduction. Finally, the total discharging duration for paraffin in case 1 is 44.5 h.

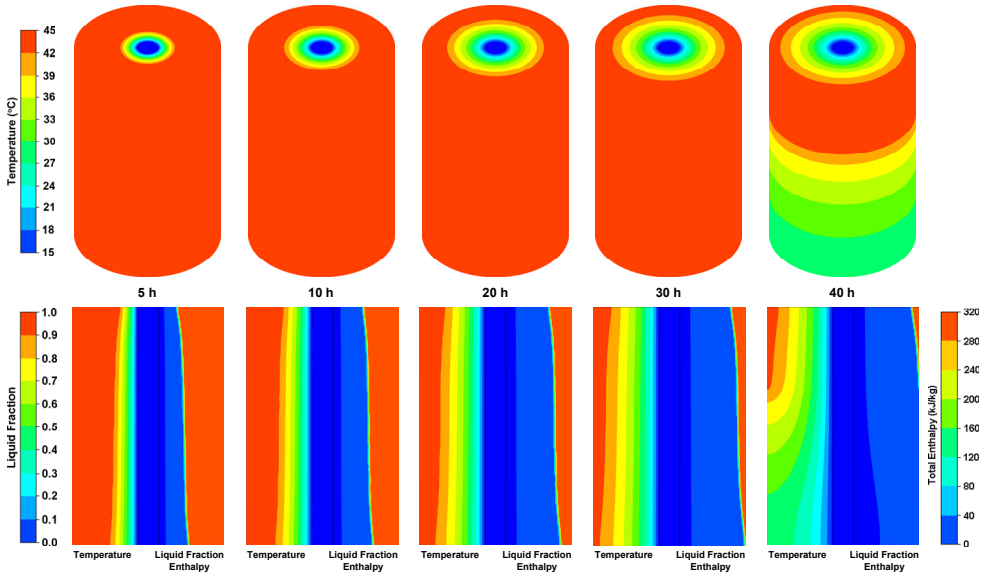

Figure 2. Temperature, total enthalpy and liquid fraction behaviour of paraffin while discharging in the shell-and-tube with no-fins (case 1).

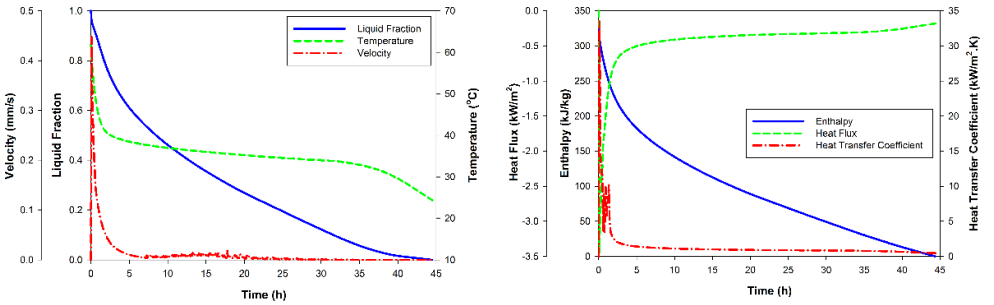

Figure 3. Transient performance of paraffin throughout the discharging cycle in the shell-and-tube with no-fins configuration (case 1).

In order to overcome the insulative behaviour of paraffin, the inclusion of GNP, longitudinal, radial and wire-wound fins are investigated in three-dimensional computational domains. The packing factor for these four scenarios (cases 2–5) are equal to 0.975, as shown in Table 2. Therefore, the comparative analyses between these thermal enhancement techniques can be conducted. Figures 4 and 5 demonstrate the thermal contours and transient responses to discharging cycles, respectively.

As compared to case 1, the inclusion of nano-additives in case 2 and extended fins in cases 3–5 have exhibited significant effectiveness in overcoming the insulative behaviour of paraffin. In case 2, the effective thermal conductivity of nano-PCM is augmented by the inclusion of 2.5% GNP. In consequence, the heat flux peaks to 3.978 kW/m^2 and the mean velocity to 0.456 mm/s. However, due to plain tube without extended fins, the thermal reach across the radial direction and accumulation of liquid nano-PCM in upper section of shell container remains similar to case 1, as shown in Figure 4a. Hence, the inclusion of nano-additives alone could not subdue all limitations incurred in case 1. Moreover, the transient variations during the discharging cycle follow similar trends as case 1, as evident from Figure 5a,b. Regardless, as compared to case 1, the total discharging duration with inclusion of nano-additives in case 2 is reduced by 39.33% to 27 h.

In the case of longitudinal fins in case 3, the resistance to the discharging cycle by the low thermal conductive paraffin is suppressed by a significant enhancement in the thermal distribution and reach in both radial and vertical directions in the shell container, as becomes evident from Figure 4b. In consequence, the heat flux and mean velocity peak to 58.79 kW/m^2 and 3.436 mm/s, as illustrated in Figure 5c,d. It can be observed from the thermal contours that the longitudinal fin design supports the buoyancy driven natural convection. Hence, the thermal gradient across the vertical direction is developed, similar to case 1 and case 2. However, due to better thermal reach and distribution by longitudinal fins, the thermal enthalpy from paraffin in the upper section of the shell container is rapidly retrieved. As a result, the total discharging duration is reduced by 88.76% to 5 h, as compared to case 1.

In case 4, the inclusion of radial fins further improves the thermal distribution and reach in both radial and vertical directions, as evident from the thermal contours in Figure 4c. However, the upward movement of liquid paraffin is hindered by radial fins, and hence, the buoyant forces-influenced natural convection is significantly reduced. In consequence, the heat flux and mean velocity curves record their peak values of 39.32 kW/m^2 and 1.964 mm/s, as shown in Figure 5e,f. It can be noticed that the confined liquid paraffin between radial fins across the vertical direction discharges the thermal enthalpy in a symmetrical manner. It suggests an improved thermal retrieval rate from paraffin, as the accumulation of liquid paraffin in upper section is avoided. As a consequence, the total discharging duration is reduced by 95.13% to 2.17 h, as compared to case 1.

Based on the merits and limitations of longitudinal and radial fins, the novel wire-wound fins configuration is designed and simulated in a three-dimensional computation domain. Although the geometrical constrains and packing factor of wire-wound fins (case 5) are similar to longitudinal fins (case 3) and radial fins (case 4), the novel design of wire-wound fins configurations generates 85.05% and 83.57% comparative enhancement in surface area for heat transfer, respectively. Therefore, due to the improved thermal distribution and reach in radial and vertical directions, along with provision for natural convection and phase front movement, the heat flux and mean velocity curves peak to 99.97 kW/m^2 and 2.168 mm/s, as shown in Figure 5g,h. Moreover, as evident from the thermal contours in Figure 4d, the thermal retrieval from paraffin in the shell container is significantly faster due to closer proximity to wire-wound fins in both vertical and radial directions. It can be noticed from the transient response of the wire-wound fins configuration that a significant portion (almost 80%) of thermal enthalpy is discharged in earlier stages (almost 20% of total duration) of the discharging cycle. Furthermore, as compared to case 1, the total discharging duration is significantly reduced by 96.44% to mere 1.58 h.

It is also confirmed that the thermal enhancement through extended fins is more effective than nano-additives in reducing the discharging duration for paraffin in computational domains with similar packing factor (case 2–5). For instance, after discharging at a similar inlet temperature for 1 h, the remaining total enthalpy in the computational domains for cases 2–5 is 243.9, 126.6, 62.13 and 12.19 kJ/kg, respectively. In other words, the total discharging duration is reduced by 81.48%, 91.96% and 94.15% for longitudinal, radial and wire-wound fins (case 3–5) as compared to case 2.

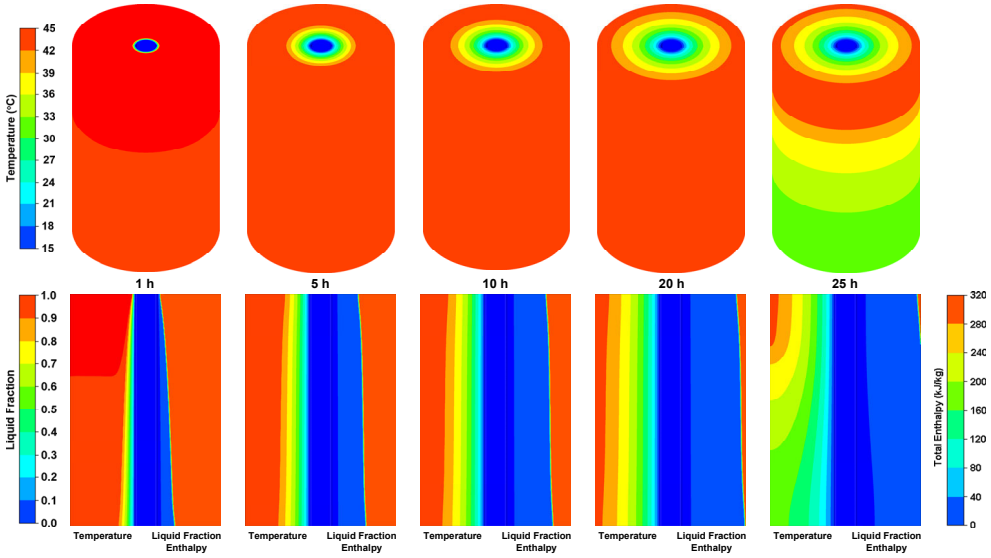

(**a**)

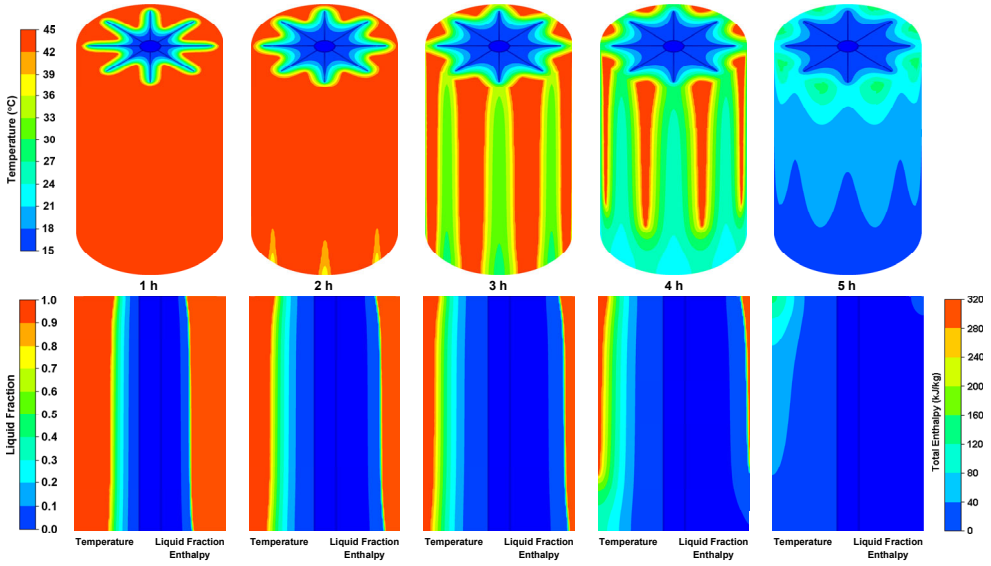

(**b**)

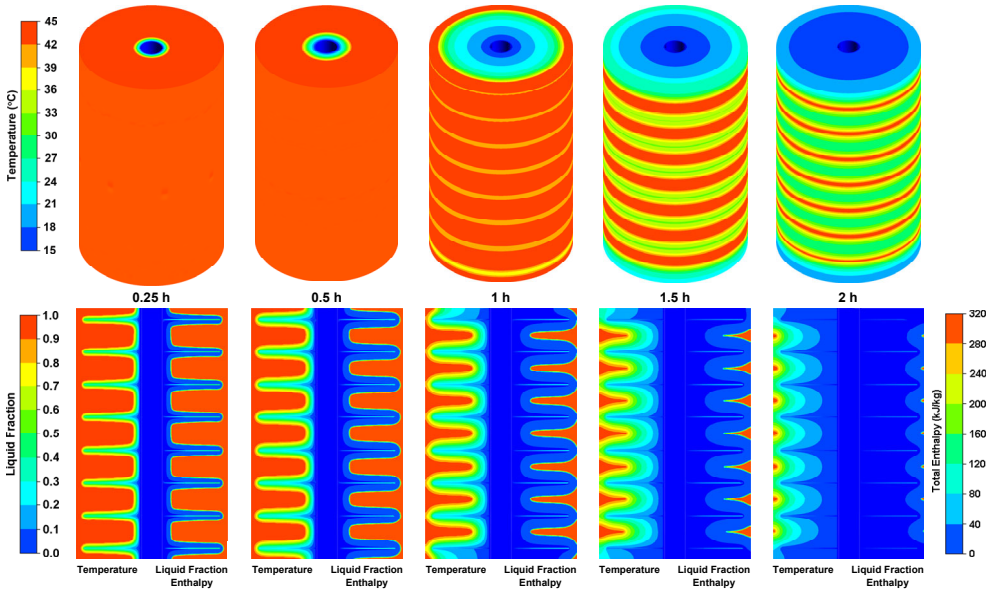

(**c**)

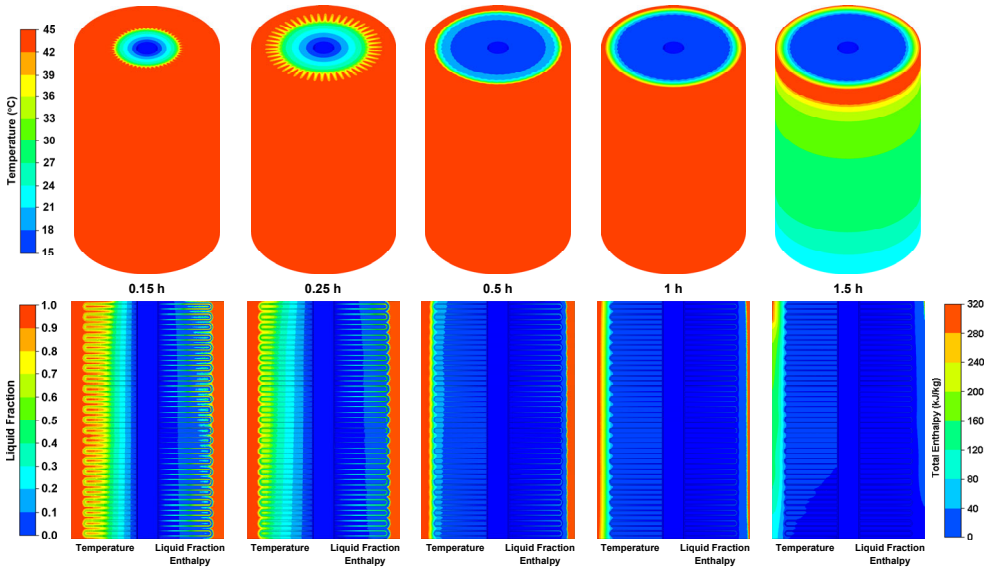

(**d**)

Figure 4. Temperature, total enthalpy and liquid fraction behaviour while discharging in the shell-and-tube with: (**a**) 2.5% GNP and no-fins (case 2), (**b**) longitudinal fins (case 3), (**c**) radial fins (case 4) and (**d**) wire-wound fins (case 5).

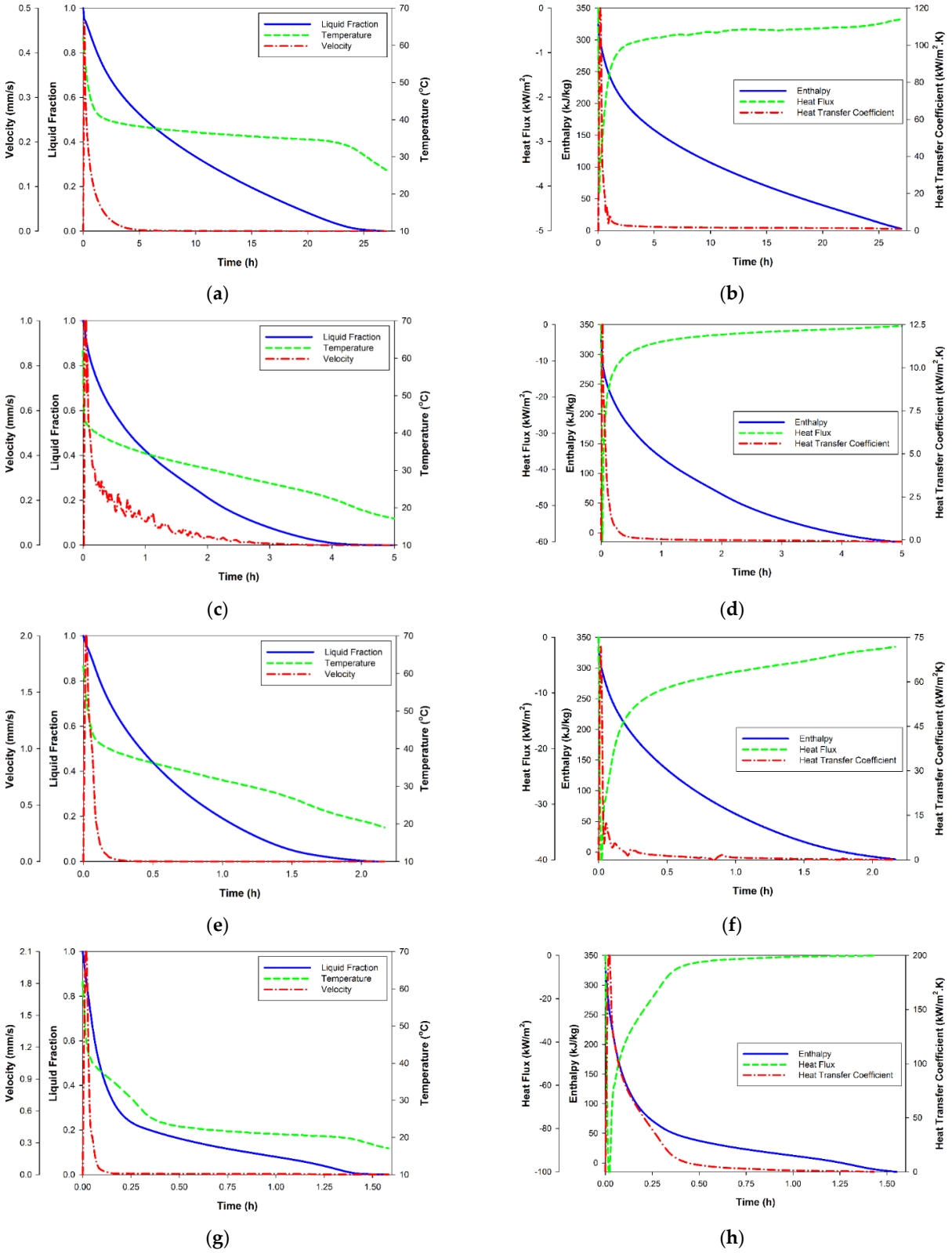

Figure 5. Transient performance of discharging cycles in shell-and-tube with: (**a**,**b**) 2.5% GNP and no-fins (case 2), (**c**,**d**) longitudinal fins (case 3), (**e**,**f**) radial fins (case 4) and (**g**,**h**) wire-wound fins (case 5).

3.2. Discharging/Solidification Cycles with Coupled Enhancement

In this section, the individual potentials of nano-additives and extended fins are combined to simulate, investigate and evaluate their effectiveness in coupled enhancement scenarios. As shown in Table 2, the coupled enhancement scenarios (cases 6–14) include longitudinal, radial and wire-wound fins with 1%, 3% and 5% GNP based nano-PCMs. In order to draw a comparison, the thermal contours and transient responses of paraffin and nano-PCMs with extended fins are presented in Figures 6 and 7.

As discussed in Section 3.1, the inclusion of nano-additives improves the effective thermal conductivity and the inclusion of extended fins augments the surface area for heat transfer, thermal reach and distribution. Hence, the coupled enhancement scenarios are expected to improve the rate of thermal enthalpy retrieval from nano-PCMs. As evident in Figure 6, the temperature and enthalpy contours illustrate an improved thermal performance for nano-PCMs with extended fins as compared to paraffin with extended fins, while discharging for 1 h. It can be noticed that the combined strengths of nano-additives and extended fins have overcome the insulative behaviour of paraffin and the accumulation of paraffin in the upper section of the shell container for longer durations. Moreover, the addition of nano-additives has adverse impacts on buoyancy-driven natural convection due to increasing the dynamic viscosity of nano-PCMs [27]. Hence, the discharging cycles in coupled enhancement scenarios are dominated by conduction heat transfer.

In the case of longitudinal fins, the inclusion of nano-additives has significantly improved the discharging rate due to augmented heat flux. The peak heat flux is increased from 58.79 kW/m^2 to 68.54, 69.22 and 70.26 kW/m^2 by replacing paraffin with 1%, 3% and 5% GNP based nano-PCMs, as shown in Figure 7a. In case of radial fins, a slight increase in peak heat flux from 39.32 kW/m^2 to 40.83, 40.98 and 42.33 kW/m^2 is noticed, as shown in Figure 7b. Similarly, in the case of wire-wound fins, the peak heat flux is slightly increased from 99.97 kW/m^2 to 104.5, 102.8 and 102 kW/m^2, as shown in Figure 7c. However, despite the slight increase, the heat flux curves for nano-PCMs with extended fins have maintained higher potential throughout the discharging cycles as compared to paraffin. Hence, the liquid fraction curves demonstrate significant reductions in the total discharging durations for the coupled enhancement scenarios, as shown in Figure 7.

In Figure 8, the total discharging durations for paraffin and nano-PCMs with extended fins are illustrated. It can be noticed that for all three extended fins, the addition of 1% GNP has demonstrated significant further reductions in total discharging durations. In the case of longitudinal fins, the discharging duration can be further reduced by 40% by employing nano-PCM instead of paraffin. Similarly, in the case of radial and wire-wound fins, the further reductions in discharging durations are 30.47% and 31.58%, respectively. Similarly, while comparing the thermal enhancement of coupled scenarios (cases 6–8) with case 1, the total discharging durations are reduced by 93.26%, 96.67% and 97.57%, respectively.

Moreover, it is evident from Figures 8 and 9 that the further increase in volume fraction from 1% to 3% and 5% has relatively minimal impact on the thermal performance enhancement of coupled scenarios. For instance, in the case of wire-wound fins, the increase in volume fraction from 1% to 3% and 5% has merely reduced the total discharging duration from 1.08 h to 1.05 and 1 h, respectively. In addition, the increase in volume fraction has adverse influence on the packing factor, and hence, on the overall capacity of total enthalpy in the shell container. For instance, the inclusion of extended fins alone has reduced the total enthalpy from 11.61 MJ (case 1) to 11.33 MJ (cases 3–5), which is further reduced to 11.15 MJ (cases 6–8), 10.79 MJ (cases 9–11) and 10.44 MJ (cases 12–14) with addition of 1%, 3% and 5% GNP-based nano-PCMs, respectively.

It can be construed that coupled heat transfer scenarios have potentials to bring about significant enhancement in reducing both charging and discharging durations of LHS systems [38]. However, it should materialise without considerable compromise on the overall capacity of total enthalpy and additional costs related to the inclusion of nano-additives

[26]. The cost evaluations of these extended fins with paraffin and nano-PCMs with different volume fractions are detailed in [38]. The novel wire-wound fin design with both paraffin and nano-PCMs has outperformed the longitudinal and radial fin configurations. In order to retrieve 11.15 MJ of thermal enthalpy, the wire-wound fin configuration (case 8) requires 63.89% and 26.97% less discharging duration compared to longitudinal (case 6) and radial fins (case 7), respectively. Hence, based on the thermo-economic performance, the wire-wound fins configuration with paraffin (case 5) and with 1% GNP based nano-PCM (case 8) are recommended as optimal candidates for large-scale utilisation of LHS systems in domestic and commercial practical applications.

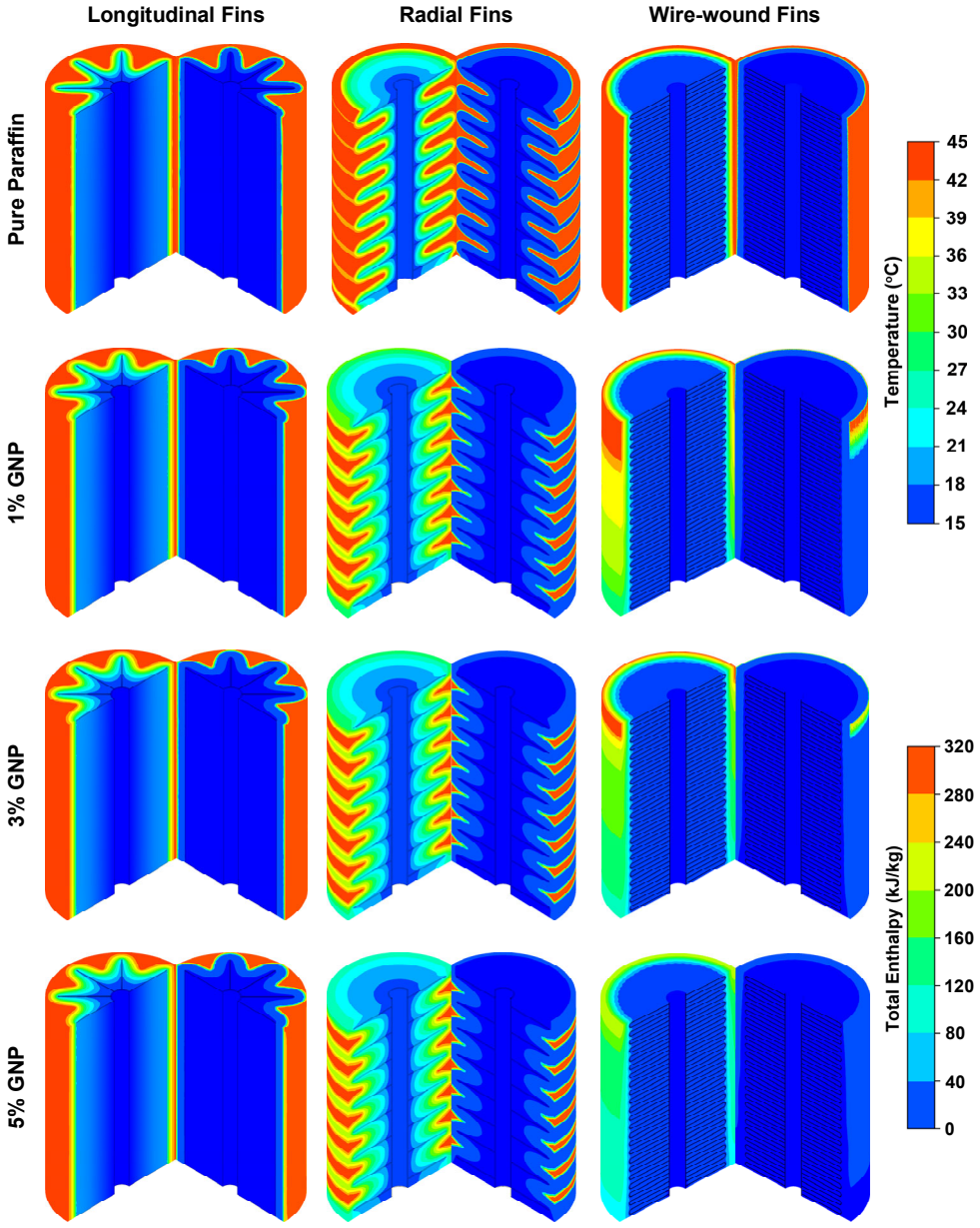

Figure 6. Temperature (**left**) and enthalpy (**right**) contours of paraffin and nano-PCMs with three varied volume fractions in longitudinal, radial and wire-wound fins configurations while discharging for 1 h.

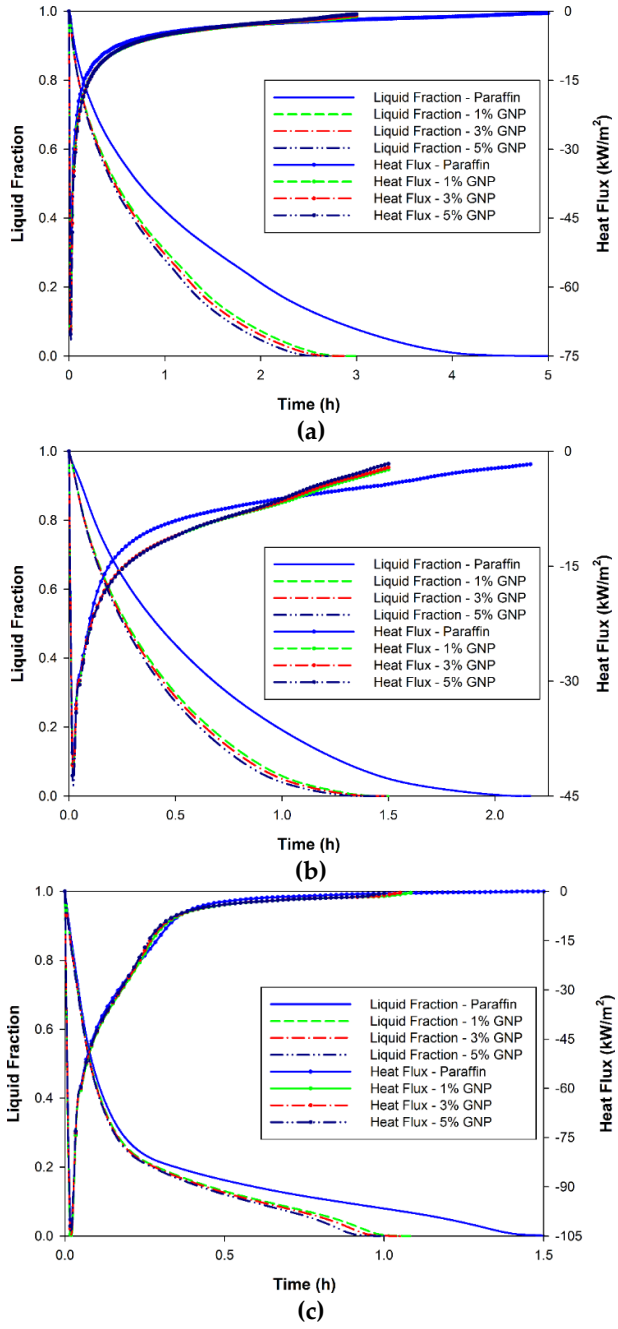

Figure 7. Transient heat flux and liquid fraction performance of paraffin and nano-PCMs while discharging in shell-and-tube with: (**a**) longitudinal, (**b**) radial and (**c**) wire-wound fins.

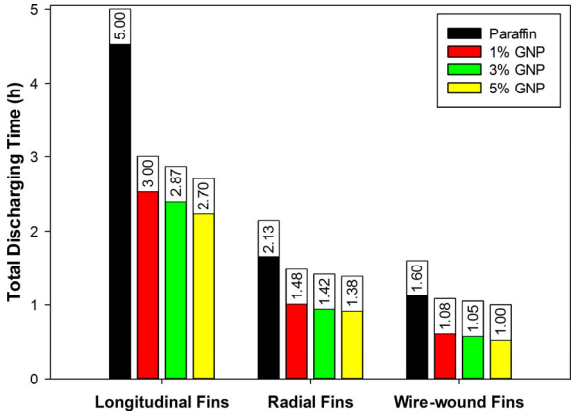

Figure 8. Total discharging time for paraffin and nano-PCMs in shell-and-tube with longitudinal, radial and wire-wound fins.

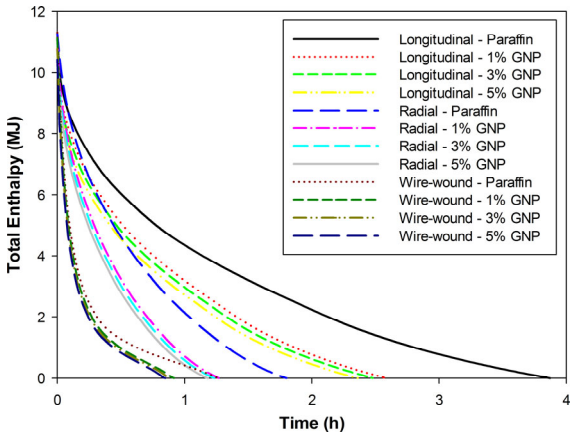

Figure 9. Total enthalpy discharged for paraffin and nano-PCMs in shell-and-tube with longitudinal, radial and wire-wound fins configurations.

4. Conclusions

In this paper, the transient numerical simulations of coupled enhancement through extended fins and nano-additives for a shell-and-tube based LHS system are conducted in three-dimensional computational domains. The extended fins include longitudinal, radial and wire-wound fins, whereas three varied volume fractions of GNP are employed as nano-additives in paraffin. Altogether, fourteen coupled enhancement scenarios are simulated to propose an optimal combination for a guaranteed higher discharging rate, enthalpy capacity and thermal distribution. The following conclusions are derived from the numerical simulations of discharging cycles:

- A discharging cycle can be categorised into three distinctive stages. In the initial stage, the sensible enthalpy is rapidly retrieved due to peak heat flux. In the second stage, the nano-PCM in close vicinity to the multi-tube passes and extended fins experience a phase change from liquid-mushy-solid while releasing the latent enthalpy. In addition, the heat flux suffers a sharp decline, followed by a gradual logarithmic reduction due to the reduced thermal gradient and increased insulative resistance by the solidified layers. In the final stage, the sensible enthalpy is released by solidified nano-PCM under sustained gradual reduction in heat flux because of the continued intensification in the insulative nature of solidified layers.
- In order to overcome the insulative behaviour, the individual influence of nano-additives and extended fins are investigated. It is noticed that extended fins are more effective than nano-additives in countering the insulative resistance and boosting the

discharging rate. For instance, the remaining total enthalpy in computational domains for cases 2–5 after discharging for 1 h are 243.9, 126.6, 62.13 and 12.19 kJ/kg, respectively. Hence, for a similar packing factor, the inclusion of longitudinal, radial and wire-wound fins has generated 81.48%, 91.96% and 94.15% higher discharging rates as compared to graphene as nano-additives.

- A novel wire-wound fins configuration is designed and simulated while considering the merits and limitations incurred by longitudinal and radial fins. Under similar geometrical constrains and packing factor values, the wire-wound fins design has developed a considerably higher fin area for heat transfer, improved thermal distribution and reach along with the provision for natural convection and phase front movement. Hence, the heat flux curve peaks to 99.97 kW/m^2 as compared to 58.79 and 39.32 kW/m^2 for longitudinal and radial fins. In similar manner, the discharging rate for wire-wound fins design is 68% and 25% higher compared to longitudinal and radial fins, respectively.
- In the case of coupled enhancement, the combined strength of nano-additives and extended fins have overcome the insulative resistance and stratification of liquid paraffin in the upper section of the shell container. For instance, the peak heat flux is increased from 58.79 to 68.54 kW/m^2 for longitudinal, 39.32 to 40.83 kW/m^2 for radial and 99.97 to 104.5 kW/m^2 for wire-wound fins configurations with inclusion of 1% GNP. As a result, the discharging rates for longitudinal, radial and wire-wound fins have further improved by 40%, 30.47% and 31.58% with inclusion of 1% GNP. However, the increase in volume fraction from 1% to 3% and 5% has produced insignificant enhancement in discharging potentials and rather adverse impacts on total enthalpy capacity. In case of wire-wound fins, the total discharging duration is slightly shortened from 1.08 h to 1.05 and 1 h, whereas the total enthalpy capacity is contracted from 11.15 MJ to 10.79 and 10.44 MJ with increasing volume fraction.
- For wider practical utilisation, the novel designed wire-wound fins with both paraffin and nano-PCMs with 1% GNP are recommended because of their significantly higher discharging potentials and insignificant reduction in total enthalpy capacity. As compared to paraffin in shell-and-tube with no-fins, the proposed wire-wound fin design with paraffin and nano-PCM has reduced the total discharging durations from 44.5 h to mere 1.60 and 1.08 h, respectively. In addition, the novel design offers flexible scalability to meet both medium- and large-scale energy storage demands, zero maintenance requirements and longer service life.

Author Contributions: Conceptualization, Z.K. and Z.A.K.; methodology, Z.K.; software, Z.K.; validation, Z.K.; formal analysis, Z.K.; investigation, Z.K.; resources, Z.A.K.; data curation, Z.K.; writing—original draft preparation, Z.K.; writing—review and editing, Z.K. and Z.A.K.; visualization, Z.K.; supervision, Z.A.K.; project administration, Z.A.K.; funding acquisition, Z.A.K. All authors have read and agreed to the published version of the manuscript.

Funding: This research was funded by National University of Sciences and Technology, Pakistan and Bournemouth University, UK, grant number 8399.

Institutional Review Board Statement: Not applicable.

Informed Consent Statement: Not applicable.

Data Availability Statement: Data is subject to confidentiality due to ongoing research.

Acknowledgments: The authors would like to acknowledge the National University of Sciences and Technology, Pakistan and Bournemouth University, UK for providing financial and in-kind support to conduct this research.

Conflicts of Interest: The authors declare no conflicts of interest.

Nomenclature

Symbol	Parameter	Unit
C	mushy zone constant	
C_p	specific heat capacity	kJ/kg K
d	diameter	m
f	liquid fraction	
$\vec{g}$	gravitational acceleration	m/s^2
H	total enthalpy	kJ
k	thermal conductivity	W/m K
k_B	Boltzmann constant	
L	latent heat capacity	kJ/kg
M_W	molecular weight	
N_A	Avogadro number	
P	pressure	N/m^2
q	heat source term	W/m^3
T	temperature	°C
t	time	(s)
V	volume	m^3
$\vec{V}$	velocity	m/s
w	weight	kg
Greek	**Parameter**	**Unit**
α	small constant value	
μ	dynamic viscosity	kg/m s
Φ_{VC}	vol fraction of nano-particles	
β	thermal expansion coefficient	1/K
ρ	density	kg/m^3
Subscripts and Acronyms		
L	liquefied phase	
S	solidified phase	
GNP	graphene nano-platelets	
HTF	heat transfer fluid	
LHS	latent heat storage	
$nPCM$	nano-PCM	
PCM	phase change material	
$P.F$	packing factor	
REF	reference	

References

1. REN21. *Renewables 2020 Global Status Report*; REN21 Secretariat: Paris, France, 2020.
2. Dudley, B. *BP Statistical Review of World Energy*; BP p.l.c.: London, UK, 2019.
3. Commission, E. *The European Green Deal*; COM/2019/640 final; European Commission: Brussels, Belgium, 2019.
4. Koohi-Fayegh, S.; Rosen, M.A. A review of energy storage types, applications and recent developments. *J. Energy Storage* **2020**, *27*, 101047.
5. da Cunha, J.P.; Eames, P. Thermal energy storage for low and medium temperature applications using phase change materials–a review. *App. Energy* **2016**, *177*, 227–238.
6. Du, K.; Calautit, J.; Wang, Z.; Wu, Y.; Liu, H. A review of the applications of phase change materials in cooling, heating and power generation in different temperature ranges. *App. Energy* **2018**, *220*, 242–273.
7. Khan, Z.; Khan, Z.; Ghafoor, A. A review of performance enhancement of PCM based latent heat storage system within the context of materials, thermal stability and compatibility. *Energy Convers. Manag.* **2016**, *115*, 132–158.
8. Al-Maghalseh, M.; Mahkamov, K. Methods of heat transfer intensification in PCM thermal storage systems. *Renew. Sustain. Energy Rev.* **2018**, *92*, 62–94.
9. Abdulateef, A.M.; Mat, S.; Abdulateef, J.; Sopian, K.; Al-Abidi, A.A. Geometric and design parameters of fins employed for enhancing thermal energy storage systems: A review. *Renew. Sustain. Energy Rev.* **2018**, *82*, 1620–1635.
10. Heat Exchangers Market by Type, Material, Application and Region. *Global Forecast* **2024**. Available online: https://www.marketsandmarkets.com/ (accessed on 8 April 2021).

11. Li, Q.; Li, C.; Du, Z.; Jiang, F.; Ding, Y. A review of performance investigation and enhancement of shell and tube thermal energy storage device containing molten salt based phase change materials for medium and high temperature applications. *App. Energy* **2019**, *255*, 113806.
12. Essa, M.A.; Rofaiel, I.Y.; Ahmed, M.A. Experimental and theoretical analysis for the performance of evacuated tube collector integrated with helical finned heat pipes using PCM energy storage. *Energy* **2020**, *206*, 118166.
13. Gil, A.; Peiró, G.; Oró, E.; Cabeza, L.F. Experimental analysis of the effective thermal conductivity enhancement of PCM using finned tubes in high temperature bulk tanks. *App. Therm. Eng.* **2018**, *142*, 736–744.
14. Abdulateef, A.M.; Mat, S.; Sopian, K.; Abdulateef, J.; Gitan, A.A. Experimental and computational study of melting phase-change material in a triplex tube heat exchanger with longitudinal/triangular fins. *Sol. Energy* **2017**, *155*, 142–153.
15. Liu, S.; Peng, H.; Hu, Z.; Ling, X.; Huang, J. Solidification performance of a latent heat storage unit with innovative longitudinal triangular fins. *Int. J. Heat Mass Transf.* **2019**, *138*, 667–676.
16. Karami, R.; Kamkari, B. Experimental investigation of the effect of perforated fins on thermal performance enhancement of vertical shell and tube latent heat energy storage systems. *Energy Convers. Manag.* **2020**, *210*, 112679.
17. Anish, R.; Joybari, M. M.; Seddegh, S.; Mariappan, V.; Haghighat, F.; Yuan, Y. Sensitivity analysis of design parameters for erythritol melting in a horizontal shell and multi-finned tube system: Numerical investigation. *Renew. Energy* **2021**, *163*, 423–436.
18. Lu, B.; Zhang, Y.; Sun, D.; Yuan, Z.; Yang, S. Experimental investigation on thermal behavior of paraffin in a vertical shell and spiral fin tube latent heat thermal energy storage unit. *Appl. Therm. Eng.* **2021**, 187, 116575.
19. Ge, R.; Humbert, G.; Martinez, R.; Attallah, M.M.; Sciacovelli, A. Additive manufacturing of a topology-optimised multi-tube energy storage device: Experimental tests and numerical analysis. *Appl. Therm. Eng.* **2020**, *180*, 115878.
20. Khan, Z.; Khan, Z.; Tabeshf, K. Parametric investigations to enhance thermal performance of paraffin through a novel geometrical configuration of shell and tube latent thermal storage system. *Energy Convers. Manag.* **2016**, *127*, 355–365.
21. Khan, Z.; Khan, Z.A. Experimental investigations of charging/melting cycles of paraffin in a novel shell and tube with longitudinal fins based heat storage design solution for domestic and industrial applications. *Appl. Energy* **2017**, *206*, 1158–1168.
22. Khan, Z.; Khan, Z.A. An experimental investigation of discharge/solidification cycle of paraffin in novel shell and tube with longitudinal fins based latent heat storage system. *Energy Convers. Manag.* **2017**, *154*, 157–167.
23. Khan, Z.; Khan, Z.A. Thermodynamic performance of a novel shell-and-tube heat exchanger incorporating paraffin as thermal storage solution for domestic and commercial applications. *Appl. Therm. Eng.* **2019**, 160, 114007.
24. Leong, K.Y.; Rahman, M.R.A.; Gurunathan, B.A. Nano-enhanced phase change materials: A review of thermo-physical properties, applications and challenges. *J. Energy Storage* **2019**, *21*, 18–31.
25. Yang, L.; Huang, J.-N.; Zhou, F. Thermophysical properties and applications of nano-enhanced PCMs: An update review. *Energy Convers. Manag.* **2020**, *214*, 112876.
26. Khan, Z.; Khan, Z.A.; Sewell, P. Heat transfer evaluation of metal oxides based nano-PCMs for latent heat storage system application. *Int. J. Heat Mass Transf.* **2019**, *144*, 118619.
27. Khan, Z.; Khan, Z.A. Experimental and numerical investigations of nano-additives enhanced paraffin in a shell-and-tube heat exchanger: A comparative study. *Appl. Therm. Eng.* **2018**, *143*, 777–790.
28. Rostami, S.; Afrand, M.; Shahsavar, A.; Sheikholeslami, M.; Kalbasi, R.; Aghakhani, S.; Shadloo, M. S.; Oztop, H. F. A review of melting and freezing processes of PCM/nano-PCM and their application in energy storage. *Energy* **2020**, *211*, 118698.
29. Goodarzi, M.; Tlili, I.; Moria, H.; Alkanhal, T.A.; Ellahi, R.; Anqi, A.E.; Safaei, M.R. Boiling heat transfer characteristics of graphene oxide nanoplatelets nano-suspensions of water-perfluorohexane (C6F14) and water-n-pentane. *Alex. Eng. J.* **2020**, *59*, 4511–4521.
30. Yarmand, H.; Gharehkhani, S.; Shirazi, S.F.S.; Goodarzi, M.; Amiri, A.; Sarsam, W.S.; Alehashem, M.S.; Dahari, M.; Kazi, S.N. Study of synthesis, stability and thermo-physical properties of graphene nanoplatelet/platinum hybrid nanofluid. *Int. Commun. Heat Mass Transf.* **2016**, *77*, 15–21.
31. Goodarzi, M.; Tlili, I.; Tian, Z.; Safaei, M.R. Efficiency assessment of using graphene nanoplatelets-silver/water nanofluids in microchannel heat sinks with different cross-sections for electronics cooling. *Int. J. Numer. Methods Heat Fluid Flow* **2019**, 30, 347–372.
32. Li, Z.X.; Khaled, U.; Al-Rashed, A.A.; Goodarzi, M.; Sarafraz, M.M.; Meer, R. Heat transfer evaluation of a micro heat exchanger cooling with spherical carbon-acetone nanofluid. *Int. J. Heat Mass Transf.* **2020**, *149*, 119124.
33. Sarani, I.; Payan, S.; Nada, S.; Payan, A. Numerical investigation of an innovative discontinuous distribution of fins for solidification rate enhancement in PCM with and without nanoparticles. *Appl. Therm. Eng.* **2020**, *176*, 115017.
34. Hosseinzadeh, K.; Moghaddam, M. E.; Asadi, A.; Mogharrebi, A.; Ganji, D. Effect of internal fins along with hybrid nano-particles on solid process in star shape triplex latent heat thermal energy storage system by numerical simulation. *Renew. Energy* **2020**, *154*, 497–507.
35. Sheikholeslami, M.; Haq, R.-U.; Shafee, A.; Li, Z. Heat transfer behavior of nanoparticle enhanced PCM solidification through an enclosure with V shaped fins. *Int. J. Heat Mass Transf.* **2019**, *130*, 1322–1342.
36. Mahdi, J.M.; Nsofor, E.C. Solidification enhancement of PCM in a triplex-tube thermal energy storage system with nanoparticles and fins. *Appl. Energy* **2018**, *211*, 975–986.
37. Singh, R.P.; Kaushik, S.; Rakshit, D. Solidification behavior of binary eutectic phase change material in a vertical finned thermal storage system dispersed with graphene nano-plates. *Energy Convers. Manag.* **2018**, *171*, 825–838.

38. Khan, Z.; Khan, Z.A. Role of extended fins and graphene nano-platelets in coupled thermal enhancement of latent heat storage system. *Energy Convers. Manag.* **2020**, *224*, 113349.
39. Rubitherm Technologies GmbH. Available online: http://www.rubitherm.eu/en/ (accessed on 1 June 2020).
40. Iolitec Ionic Liquids Technologies GmbH. Available online: https://iolitec.de/en (accessed on 1 June 2020).
41. Gray, D.D.; Giorgini, A. The validity of the Boussinesq approximation for liquids and gases. *Int. J. Heat Mass Transf.* **1976**, *19*, 545–551.
42. Nield, D.A.; Bejan, A.; Nield-Bejan. *Convection in Porous Media*; Springer: Berlin/Heidelberg, Germany, 2006; Volume 3.
43. Mahdi, J.M.; Lohrasbi, S.; Ganji, D.D.; Nsofor, E.C. Accelerated melting of PCM in energy storage systems via novel configuration of fins in the triplex-tube heat exchanger. *Int. J. Heat Mass Transf.* **2018**, *124*, 663–676.
44. Corcione, M. Empirical correlating equations for predicting the effective thermal conductivity and dynamic viscosity of nanofluids. *Energy Convers. Manag.* **2011**, *52*, 789–793.
45. Kandasamy, R.; Wang, X.-Q.; Mujumdar, A. S. Transient cooling of electronics using phase change material (PCM)-based heat sinks. *Appl. Therm. Eng.* **2008**, *28*, 1047–1057.
46. Vajjha, R.S.; Das, D.K. Experimental determination of thermal conductivity of three nanofluids and development of new correlations. *Int. J. Heat Mass Transf.* **2009**, *52*, 4675–4682.
47. Maxwell, J.C. *A Treatise on Electricity and Magnetism*; Clarendon Press: Oxford, UK, 1881; Volume 1.